RESEARCH ARTICLE

Numerical Study of Nonlinear Third-Grade Nanofluid with Generalized Heat and Mass Flux in Mixed Convective Flow

Faisal Shah[1,2,*]

[1] Research Centre of Fluid Machinery Engineering and Technology, Jiangsu University, Zhenjiang 212013, China
[2] Department of Mathematics, Quaid-i-Azam University, Islamabad 44000, Pakistan

Abstract

This paper investigates the bio-convective behavior of a third-grade non-Newtonian nanofluid over a stretching sheet. While the influence of Newtonian fluid flow based on classical Fourier and Fick's laws has been widely discussed in previous studies, this work focuses on a novel third-grade nanofluid model incorporating various physical effects. Notably, the classical Fourier law is replaced by the Cattaneo–Christov (CC) theory for both heat and mass fluxes, capturing relaxation phenomena in the presence of bioconvective effects. Heat and mass transport are modeled using the CC framework, and nanoscale mechanisms are described via the Buongiorno nanofluid model. The influences of thermophoresis and Brownian motion are analyzed alongside dissipative and radiative effects. The Optimal Homotopy Asymptotic Method (OHAM) is employed to solve the resulting nonlinear equations. Graphical representations of key parameters are presented. Results reveal that the velocity profile increases with higher values of material parameters but decreases with an increase in the Reynolds number. The temperature decreases with higher Prandtl number but increases with greater radiation parameter. The concentration profile is found to decline with increasing Schmidt number.

Keywords: modified fourier and fick's law, third-grade nano-fluid, MHD, viscous dissipation.

1 Introduction

Third grade (3rd) fluid is a subcategory of differential types that can explain the impacts of both shear thickening and thinning phenomena. The stability of third grade (3rd) liquid is explored by Fosdick and Rajagopal [1]. Viscoelastic mixed convective flow is developed by Mastroberardino [1] caused by stretchable surfaces. The study of thermodynamics for the third grade (3rd) liquid with heat generation has been done by Adesanya and Makinde [2]. Ellahi and Riaz [3] systematically thought about third grade (3rd) fluid flow with variable viscosity. Third grade squeezing flow is securitized by Hayat et al. [4]. Sajid et al. [5] investigated the coating process of a non-Newtonian material. Hayat et al. [6] evaluate

Submitted: 07 May 2025
Accepted: 21 June 2025
Published: 03 August 2025

Vol. 1, **No.** 2, 2025.
10.62762/JAM.2025.671250

***Corresponding author:**
✉ Faisal Shah
sfaisal@math.qau.edu.pk

Citation
Shah, F. (2025). Numerical Study of Nonlinear Third-Grade Nanofluid with Generalized Heat and Mass Flux in Mixed Convective Flow. *ICCK Journal of Applied Mathematics*, 1(2), 52–61.

Soret Dufour's effects on third-grade fluid.

Nomenclature

$\mathbf{u}$	Velocity component along x-axis
$\mathbf{v}$	Velocity component along y-axis
$\mathbf{a}$	Stretching/shrinking constant
$\mathbf{g}$	Gravity
$\mathbf{B_0}$	Magnetic field constant
$\mathbf{T}$	Temperature
$\mathbf{T_w}$	Temperature of the wall
$\mathbf{T_\infty}$	Ambient temperature of the nanofluid
$\mathbf{C_\infty}$	Ambient concentration of the hybrid nanofluid
$\rho_\mathbf{f}$	Density of the fluid
ε	Drag coefficient
$\nu_\mathbf{f}$	Kinematic viscosity of the base fluid
$\mu_\mathbf{f}$	Viscosity of the fluid
$\mathbf{k}^*$	Porous medium permeability
$\mathbf{Q}$	Heat generation rates
$\mathbf{D_B}$	Brownian motion
$\mathbf{k}^*$	Absorption coefficient
$\mathbf{D_T}$	Thermophoresis variable
α_1,α_2,α_3	Material constant for third grade fluid
σ^*	Stefan Boltzmann constant
$\mathbf{t}$	Dimensionless temperature
ζ	Similarity variable
$\mathbf{q_r}$	Radiative heat flux
Pr	Prandtl number
$\mathbf{R_d}$	Radiation variable
$\mathbf{M}$	Magnetic parameter
α_1^*,α_2^*,α_3^*	Material Parameter for third grade fluid
$\mathbf{M}$	Magnetic parameter
$\alpha_\mathbf{f}$	Thermal diffusivity
$\mathbf{S}$	Ratio of rates
$\mathbf{N_B}$	Brownian motion parameter
$\mathbf{Sc}$	Schmidt number
$\mathbf{N_T}$	Thermophoresis parameter
δ	Heat generation parameter
λ	Mixed convection parameter
$\mathbf{Ec}$	Eckert number
γ	Thermal relaxation variable
γ_1	Solutal relaxation parameter
$\mathbf{C_f}$	Skin friction coefficient
$\mathbf{Re_x}$	Reynold number

Nano fluids are produced by dispersing solid particles of a nano-meter size into various conventional liquids such as water, gasoline and ethylene glycol respectively. Nano-liquids have numerous applications in manufacturing and automotive cooling, sensing, production of new types of fuels, microelectronic cooling, hybrid-powered engine efficiency and home appliance heating/cooling etc. Choi [7] discovered the term nano fluid. The infusion of metallic nano particles hooked on conventional liquids would greatly improve the thermal efficiencies of those liquids as explained by him. The Nano fluid convective transportation model with the Brownian and thermophoresis effects was analysed by Buongiorno [8]. Non-effective Prandtl numbers by considering nanoparticles and entropy analysis are researched by Hayat et al. [9]. Entropy optimization with different fluid models is studied by Ahmad et al. [10].

Fourier heat conduction expression [11] give much information about heat transfer through the flux. The paradox of heat conduction is leads by this expression. The Cattaneo [12] has revised the relation of thermal relaxation time. Suggestions about the Oldroyed upper convected derivatives should be considered in Ref. [13, 14] instead of material differentiations are given by Christov. Thermal variability in a porous medium by the retentive Cattaneo-Christov (CC) model is analysed by Haddad [15]. The impact of Cattaneo-Christov model considering different fluid models is discussed by some researchers [16–19].

Here, third grade (3rd) nano liquid flow towards a stretchable sheet is discussed. Bio-convection, radiative heat, dissipative impacts and heat generation are also discussed. By using the optimal method [20–23] obtained the analytical solution of the governing equations. The results for various physical variables are discussed through graphs.

The simultaneous study of generalized (non-Fourier, non-Fick) heat and mass flux conditions inside a mixed convective flow regime and nonlinear third-grade nanofluid behavior is what makes this work innovative. The integration of third-grade fluids and nanofluid dynamics under nonlinear rheological behavior has not been extensively studied, particularly when generalized boundary conditions that take into consideration thermal and solutal relaxation effects are present. Furthermore, by considering both buoyancy-driven and forced convective effects both of which are crucial in real-world applications including industrial heat exchangers, biomedical flows, and electronic device cooling—this work integrates a realistic description of mixed convection.

2 Physical Model

In this study, a two-dimensional (x, y) incompressible non-Newtonian fluid flow over a stretching sheet is considered. Both mixed convection and bioconvective effects are taken into account. The sheet is stretched along the x-axis with a linear stretching velocity $U_w = ax$. The surface temperature and concentration are denoted by T_w and C_w, respectively, while T_∞ and C_∞ represent the ambient temperature and concentration

far from the surface. The free stream velocity outside the boundary layer is represented by U_e. The schematic diagram of the flow configuration is illustrated in Figure 1.

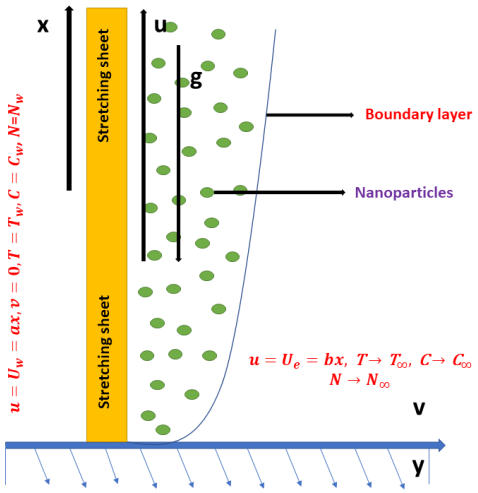

Figure 1. Flow geometry.

3 Formulation of governing equations

In this work, a mixed convective, laminar, two-dimensional flow over a moving surface is investigated. The analysis incorporates a third-grade non-Newtonian fluid model in the presence of gyrotactic micro-organisms. Heat and mass transport are examined using the Cattaneo–Christov (CC) flux model, which accounts for relaxation effects beyond the classical laws. Furthermore, the influences of Brownian motion and thermophoresis are considered to capture nanoscale transport phenomena. Thermal radiation and viscous dissipation are included as additional heat sources in the energy equation. The governing equations relevant to this study are presented below.

$$\frac{\partial u}{\partial x} + \frac{\partial v}{\partial y} = 0, \tag{1}$$

$$\left.\begin{array}{c} u\frac{\partial u}{\partial x} + v\frac{\partial u}{\partial y} = U_e\frac{\partial U_e}{\partial x} + \frac{\alpha_1}{\rho}\left(\frac{\partial u}{\partial x}\frac{\partial^2 u}{\partial y^2} + u\frac{\partial^3 u}{\partial x\partial y^2} + 3\frac{\partial u}{\partial y}\frac{\partial^2 u}{\partial x\partial y} + v\frac{\partial^3 u}{\partial y^3}\right) \\ +\frac{\alpha_2}{\rho}\left(2\frac{\partial u}{\partial y}\frac{\partial^2 u}{\partial x\partial y}\right) + 6\frac{\alpha_3}{\rho}\left(\left(\frac{\partial u}{\partial y}\right)^2\frac{\partial^2 u}{\partial y^2}\right) + g\beta_t(T - T_\infty) + g\beta_t(C - C_\infty) \\ \frac{\sigma Q_o Q_o}{\rho a}u + \nu\frac{\partial^2 u}{\partial y^2} \end{array}\right\}, \tag{2}$$

The relevant periphery conditions are:

$$\left.\begin{array}{c} u = U_w = ax,\ v = 0\ at\ y = 0, \\ u = U_e = bx \text{ when } y \to \infty \end{array}\right\}. \tag{3}$$

Drag force is:

$$C_{fx} = \left(\frac{\tau_w}{\rho_f\,(U_w)^2}\right), \tag{4}$$

here:

$$\tau_w = \left(\mu\frac{\partial u}{\partial y}\right)_{y=0} + \left[\frac{\alpha_1}{\rho}\left(u\frac{\partial^2 u}{\partial x\partial y} + 2\frac{\partial u}{\partial x}\frac{\partial u}{\partial y} + v\frac{\partial^2 u}{\partial y^2}\right) + 2\frac{\alpha_3}{\rho}\left(\frac{\partial u}{\partial y}\right)^3\right]_{y=0}. \tag{5}$$

The energy and concentration expression for Cattaneo-Christove (CC) model are:

$$\left.\begin{array}{c} u\frac{\partial T}{\partial x} + v\frac{\partial T}{\partial y} + \delta_E\Omega_E = \alpha\frac{\partial^2 T}{\partial y^2} + \tau\left[D_B\frac{\partial C}{\partial y}\frac{\partial T}{\partial y} + \frac{D_T}{T_\infty}\left(\frac{\partial T}{\partial y}\right)^2\right] \\ +\frac{Q}{\rho C_p}(T - T_\infty) - \frac{16\sigma^* T^3}{3\rho c_p k_1}\frac{\partial^2 T}{\partial y^2} + \frac{\mu}{\rho C_p}\left(\frac{\partial u}{\partial y}\right)^2 \\ +\frac{\alpha_1}{\rho C_p}\left[\left(u\frac{\partial u}{\partial y}\frac{\partial^2 u}{\partial x\partial y} + v\frac{\partial u}{\partial y}\frac{\partial^2 u}{\partial y^2}\right)\right] + 2\frac{\alpha_3}{\rho C_p}\left(\frac{\partial u}{\partial y}\right)^4 \end{array}\right\}, \tag{6}$$

here Ω_E is given by:

$$\left.\begin{array}{c} \Omega_E = u\frac{\partial u}{\partial x}\frac{\partial T}{\partial x} + v\frac{\partial u}{\partial y}\frac{\partial T}{\partial y} + u\frac{\partial v}{\partial x}\frac{\partial T}{\partial y} + v\frac{\partial u}{\partial y}\frac{\partial T}{\partial x} + 2uv\frac{\partial^2 T}{\partial y\partial x} + u^2\frac{\partial^2 T}{\partial x^2} + v^2\frac{\partial^2 T}{\partial y^2} \\ -\frac{Q}{\rho C_p}\left(u\frac{\partial T}{\partial x} + v\frac{\partial T}{\partial y}\right) - \frac{\mu}{\rho C_p}\left(2u\frac{\partial u}{\partial y}\frac{\partial^2 u}{\partial x\partial y} + 2v\frac{\partial u}{\partial y}\frac{\partial^2 u}{\partial y^2}\right) \\ +\frac{\alpha_1}{\rho C_p}\left[\begin{array}{c} u^2\left(\frac{\partial^2 u}{\partial x\partial y}\frac{\partial^2 u}{\partial x\partial y} + \frac{\partial u}{\partial y}\frac{\partial^3 u}{\partial x^2\partial y}\right) + 2uv\left(\frac{\partial u}{\partial y}\frac{\partial^2 u}{\partial x\partial y} + \frac{\partial u}{\partial y}\frac{\partial^3 u}{\partial x\partial y^2}\right) \\ +v^2\left(\frac{\partial^2 u}{\partial y^2}\frac{\partial^2 u}{\partial y^2} + \frac{\partial u}{\partial y}\frac{\partial^3 u}{\partial y^3}\right) \end{array}\right] \\ +\frac{\alpha_3}{\rho C_p}\left(4u\frac{\partial u}{\partial y}\frac{\partial^2 u}{\partial x\partial y} + uv\frac{\partial u}{\partial y}\frac{\partial^2 u}{\partial y^2}\right) - \tau D_B\left(\begin{array}{c} v\frac{\partial T}{\partial y}\frac{\partial^2 C}{\partial y^2} + v\frac{\partial C}{\partial y}\frac{\partial^2 T}{\partial y^2} + \\ u\frac{\partial^2 C}{\partial x\partial y}\frac{\partial T}{\partial y} + u\frac{\partial C}{\partial y}\frac{\partial^2 T}{\partial x\partial y} \end{array}\right) \\ +2\frac{\tau D_T}{T_\infty}\left(v\frac{\partial T}{\partial y}\frac{\partial^2 T}{\partial y^2} + u\frac{\partial T}{\partial y}\frac{\partial^2 T}{\partial x\partial y}\right) + R_d\left(u\frac{\partial^2 T}{\partial x\partial y} + v\frac{\partial^2 T}{\partial y^2}\right) \end{array}\right\}. \tag{7}$$

$$u\frac{\partial C}{\partial x} + v\frac{\partial C}{\partial y} + \delta_F\Omega_F = D_B\frac{\partial^2 C}{\partial y^2} + \frac{D_T}{T_\infty}\frac{\partial^2 T}{\partial y^2}\Bigg\}, \tag{8}$$

here Ω_F is given as:

$$\left.\begin{array}{c} \Omega_F = u^2\frac{\partial^2 C}{\partial x^2} + u\frac{\partial u}{\partial x}\frac{\partial C}{\partial x} + u\frac{\partial v}{\partial x}\frac{\partial C}{\partial y} + 2uv\frac{\partial^2 C}{\partial x\partial y}\frac{\partial T}{\partial x} + v\frac{\partial u}{\partial y}\frac{\partial C}{\partial x} + v^2\frac{\partial^2 C}{\partial y^2} + \\ v\frac{\partial v}{\partial y}\frac{\partial C}{\partial y} - D_B\left(u\frac{\partial^3 C}{\partial x\partial y^2} + v\frac{\partial^3 C}{\partial y^3}\right) - \frac{D_T}{T_\infty}\left(v\frac{\partial^3 T}{\partial y^3} + u\frac{\partial^3 T}{\partial x\partial y^2}\right) \end{array}\right\}. \tag{9}$$

The relevant conditions are:

$$\left.\begin{array}{c} T \to T_w \text{ at } y = 0, \\ T \to T_\infty \text{ when } y \to \infty, \end{array}\right\}. \tag{10}$$

$$\left.\begin{array}{c} C \to C_w \text{ at } y = 0, \\ C \to C_\infty \text{ at } y \to \infty, \end{array}\right\}. \tag{11}$$

In above equation D_B,D_T denotes Brownian and thermosphere quantity, $(Q > 0)$ be the heat generation rate, the Boltzmann constant is σ^*, k_1 denote the coefficient of mean absorption and the specific heat is the C_p.

4 Non-Dimensional formulation

Considering transformations:

$$\left.\begin{array}{l} u = axf'(\eta),\ v = -\sqrt{a\nu}f(\eta),\ t = \dfrac{T-T_\infty}{T_w-T_\infty},\ J = \dfrac{C-C_\infty}{C_w-C_\infty}, \\ \eta = \sqrt{\dfrac{a}{\nu}}y \end{array}\right\}, \tag{12}$$

the eq. (1) is satisfied while others eqs. (2)-(11) are:

$$\left.\begin{array}{c} f''' + ff'' - f'^2 + \alpha_1^*\left(f'f''' - f'f'''' - f''''f\right) + \left(\alpha_1^* + \alpha_2^*\right)f''f'' \\ +6\alpha_3^* Ref''f''f'''' + S^2 + Mf' + \lambda t + \lambda\lambda_c J = 0 \end{array}\right\}, \tag{13}$$

$$\left.\begin{array}{c} (1+R_d)t'' + \Pr*\gamma_1*\left(ff't' + f'f't'' - \delta ft' - 2fft''\right) + Prft' \\ \Pr*\gamma_1*Ec*\left(2f'f'f''' - ff''f''''\right) - \Pr*\gamma_1*N_B*(ff'J'' - fJ't') + \Pr*Ec*\alpha_1^* \\ f'f''f'' + \Pr*\gamma_1*Ec*\alpha_1^*\left(\begin{array}{c} f'f'f'' + ff''f'' - ff'f'f''' \\ -2fff'''f''' + fff'f'' \end{array}\right) + \Pr*Ec*f''f'' \\ \Pr*\gamma_1*Ec*\alpha_3^**\left(4ff''f'' + ff''f''''\right) + \Pr*Ec*\alpha_1^**ff''f''' + 2\Pr*Ec*\alpha_3^**Re \\ f''f''f''f'' - \Pr\gamma_1 N_t J''t' - \Pr\gamma_1 R_d ft'' + N_B t'J' + N_t t't' + \Pr\delta t] = 0, \end{array}\right\} \tag{14}$$

$$\left.J'' + LefJ' + \frac{N_B}{N_t}t'' - Le\gamma_2[f^2J'' + ff'J'] - \gamma_2\frac{N_B}{N_t}t'' = 0\right\}, \tag{15}$$

$$\left\{\begin{array}{c} f(0) = 0,\ t(0) = 1, f'(0) = 1, J(0) = 1 \\ f'(\infty) = S,\ t(\infty) = 0,\ J(\infty) = 0, \end{array}\right\}. \tag{16}$$

Dimensionless form of skin friction is given as:

$$\sqrt{Re_x}C_{fx} = f''(0) + \alpha_1^*\left(3f'(0)f''(0) - f(0)f'''(0)\right) + \alpha_2^*\left(f''(0)\right)^3. \tag{17}$$

where $\Pr\left(=\frac{\mu C_p}{k}\right)$ is Prandtl number, Hartman number $M\left(=\frac{\sigma M_o M_o}{\rho a}\right)$, ratio of rates is the $S\left(=\frac{b}{a}\right)$, thermophoresis parameter $N_t\left(=\frac{\tau D_T(T_w-T_\infty)}{\nu T_\infty}\right)$, the radiation parameter is $R_d\left(=\frac{16\sigma^*T_\infty^3}{3k_1k}\right)$, Schmidt number is $Sc\left(=\frac{\nu}{D_B}\right)$, Brownian motion parameter $N_B\left(=\frac{\tau D_B(C_w-C_\infty)}{\nu}\right)$, the third grade fluid parameters are $\left(\alpha_1^*\left(=\frac{\alpha_1 a}{\mu}\right), \alpha_2^*\left(=\frac{\alpha_2 a}{\mu}\right), \alpha_3^*\left(=\frac{\alpha_3 a}{\mu}\right)\right)$, heat generation parameter $\delta\left(=\frac{Q}{\rho C_p}\right)$, $\lambda\left(=\frac{g\beta_t(T_w-T_\infty)}{a}\right)$ mixed convective parameter, Eckert number is $Ec(=\frac{U_w^2}{C_p(T_w-T_\infty)})$, thermal relaxation parameter $\gamma(=a\delta_E)$ and solutal concentration parameter $\gamma_1(=a\delta_F)$.

5 Methodology

We determined the series solutions by using homotopy analysis:

$$\varepsilon_{k^*}^f(h_f) = \frac{1}{N^*+1}\sum_{j^*=0}^{N^*} * \left[\sum_{i=0}^{k} *(f_i)_{\eta=j^*\Pi\eta}\right]^2, \tag{18}$$

$$\varepsilon_{k^*}^t(h_f,h_t,h_J) = \frac{1}{N^*+1} * \sum_{j^*=0}^{N^*} * \left[\sum_{i=0}^{k^*} *(f_i)_{\eta=j^*\Pi\eta}, \sum_{i=0}^{k^*} *(t_i)_{\eta=j^*\Pi\eta}, \sum_{i=0}^{k^*} *(J_i)_{\eta=j^*\Pi\eta}\right]^2, \tag{19}$$

$$\varepsilon_{k^*}^J(h_f,h_t,h_J) = \frac{1}{N^*+1}\sum_{j^*=0}^{N^*} * \left[\sum_{i=0}^{k^*} *(f_i)_{\eta=j^*\Pi\eta}, \sum_{i=0}^{k^*} *(t_i)_{\eta=j^*\Pi\eta}, \sum_{i=0}^{k^*} *(J_i)_{\eta=j^*\Pi\eta}\right]^2, \tag{20}$$

$$\varepsilon_{k^*}^{t^*} = \varepsilon_{k^*}^f + \varepsilon_{k^*}^t + \varepsilon_{k*}^J, \tag{21}$$

where the total square residual error is represented by $\varepsilon_{k*}^{t^*}$. When $S = 0.1$, $M = 0.2$, $\Pr = 1.2$, $N_B = 0.5$, $\alpha_1^* = 0.1$, $\alpha_2^* = 0.2$, $N_T = 0.1$, $\alpha_1^* = 0.3$, $\gamma = \gamma_1 = 0.2$, $Re = 0.1$, $Ec = 1.0$, $\lambda = 0.1$ and $Da^{-1} = 0.4$. Then the total usual squared residual error is abated by employing Mathematica BVPh2.0. The optimal values of convergence control variables are $h_f = -0.816767$, $h_t = -0.287548$, $h_J = 2.35602$, and $h_\phi = -0.4562$,. The total residual error is $\varepsilon_{k^*}^{t^*} = 0.79552$. The variation of the total residual error with respect to the approximation order is illustrated in Figure 2.

6 Discussion

6.1 Velocity Distribution:

Figure 3 illustrates the variation of the magnetic parameter (M) on $f'(\eta)$, where $f'(\eta)$ increases with

Table 1. Residual errors.

$\mathbf{k}^*$	$\varepsilon^{\mathbf{f}}_{\mathbf{k}^*}$	$\varepsilon^{\mathbf{t}}_{\mathbf{k}^*}$	$\varepsilon^{\mathbf{J}}_{\mathbf{k}^*}$
2	0.346508	0.016186	0.0881337
4	0.0326625	0.00574157	0.0198452
8	0.307458	0.00163756	0.00411318
10	0.300818	0.00104241	0.002397
12	0.029512	0.000708731	0.00159226
14	0.0290089	0.000506021	0.00119825

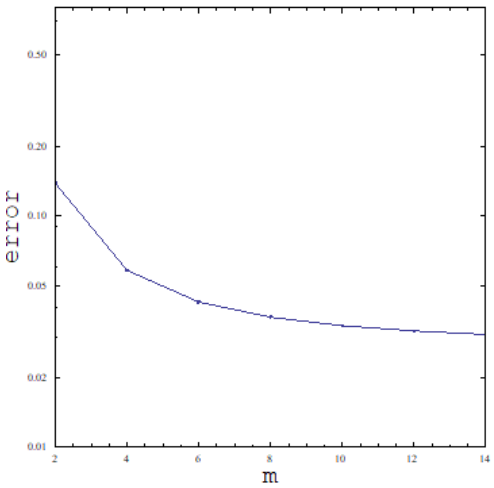

Figure 2. Total residual error.

$M = 0.0, 0.1, 0.2, 0.3, 0.4, 0.5$. Because magnetic field produces resistive forces between fluid elements therefore reduces velocity. Figures 4, 5, and 6 illustrate the influence of α_1^*, α_2^* and α_3^* respectively on velocity profile. It displays that a inverse inclination is followed by a transition at $\eta = 1.5$ when increase of $(\alpha_1^* = 1.0, 2.0, 3.0, 4.0, 5.0, 6.0)$ liquid velocity trivializes adjacent the plate. On the fact material variables are converse relation to viscosity. So, increase in $(\alpha_2^* = 1.0, 2.0, 3.0, 4.0, 5.0, 6.0)$ and $(\alpha_3^* = 1.0, 2.0, 3.0, 4.0, 5.0, 6.0)$ moderate the fluid viscosity down and thus augment the liquefied motion. Figure 7 illustrates the influence of the Reynolds number $(Re = 1.0, 2.0, 3.0, 4.0, 5.0, 6.0)$ on the velocity profile $f'(\eta)$. It is observed that the fluid velocity $f'(\eta)$ decreases as the Reynolds number increases. Figure 8 presents the variation of $f'(\eta)$ with respect to the ratio parameter S. As S increases, the fluid velocity also increases. This is because a higher value of S corresponds to a stronger ambient flow, which enhances the overall fluid motion. The effect of the stretching parameter λ on the velocity $f'(\eta)$ is shown in Figure 9. For higher of (λ) the $f'(\eta)$ enhances. Physically viscous forces reduce for greater estimation of (λ) and so velocity improves.

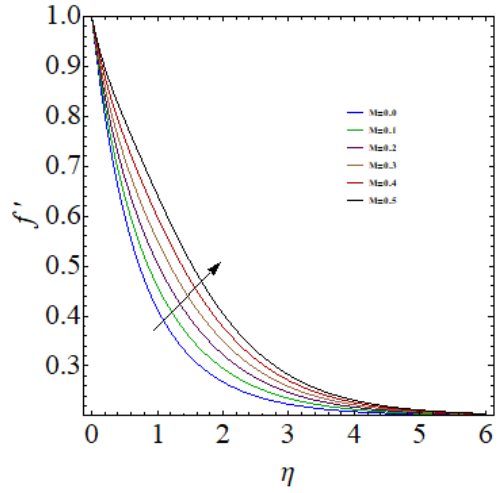

Figure 3. f' via M.

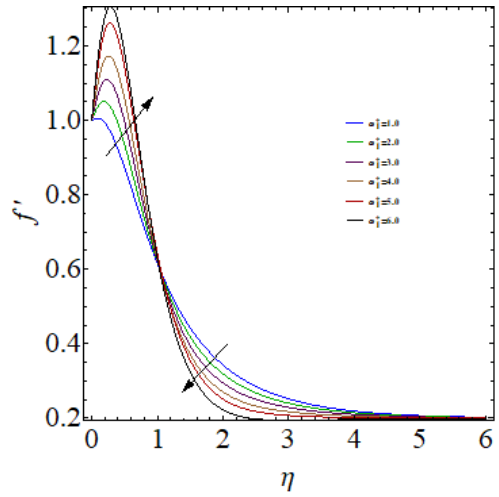

Figure 4. f' via α_1^*.

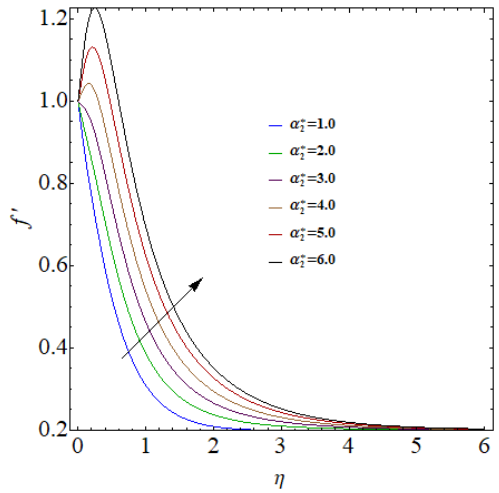

Figure 5. f' via α_2^*.

6.2 Temperature Distribution:

Figure 10 examines the effect of the thermal generation parameter $\delta = 0.1, 0.2, 0.3, 0.4, 0.5, 0.6$ on the temperature profile $t(\eta)$, showing that temperature

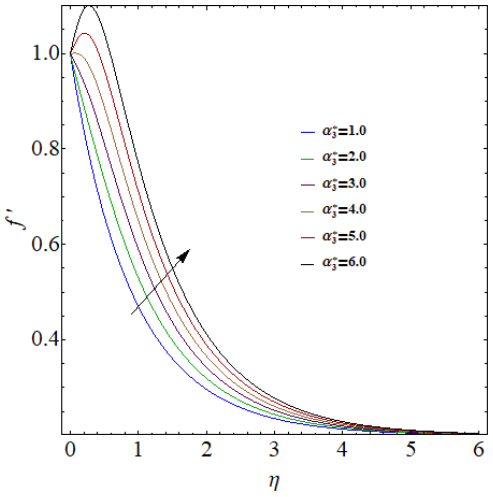

Figure 6. f' via α_3^*.

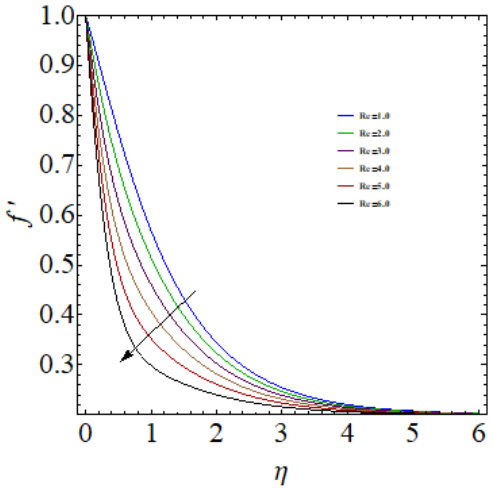

Figure 7. f' via Re.

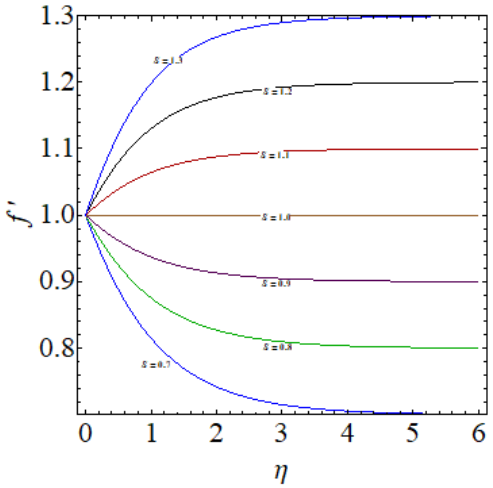

Figure 8. f' via S.

increases as δ increases due to enhanced heat generation. Figures 11 and 12 indicate that higher values of the material parameters α_2^* and α_3^*, which represent normal stresses and viscous forces, lead to a decrease in temperature; this occurs because

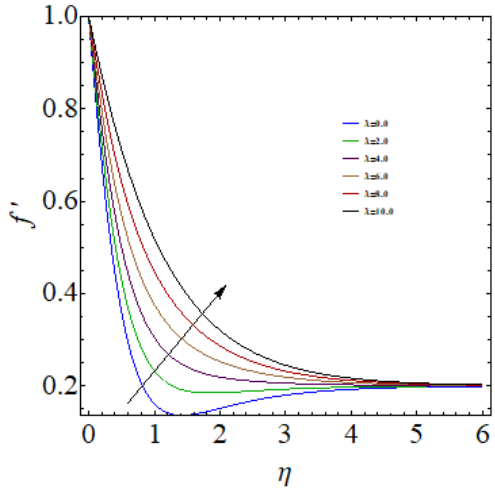

Figure 9. f' via λ.

stronger material parameters reduce viscous forces while increasing normal stresses. Figure 13 reveals that a larger Prandtl number Pr results in a lower temperature profile, since higher Pr values correspond to reduced thermal diffusivity, thereby limiting heat transfer from hot to cold regions. The influence of the radiation parameter R_d on $t(\eta)$ is shown in Figure 14, where increasing R_d enhances radiative heat transfer and raises the temperature. Figure 15 demonstrates that the temperature rises with higher Eckert number Ec, as more kinetic energy is converted into internal energy. Figure 16 highlights the role of the heat relaxation parameter $\gamma = 0.0, 1.0, 2.0, 3.0, 4.0, 5.0$, showing that larger γ values delay heat transfer, leading to reduced temperature. Lastly, Figure 17 shows that an increase in the Brownian motion parameter N_B contributes to a higher temperature profile.

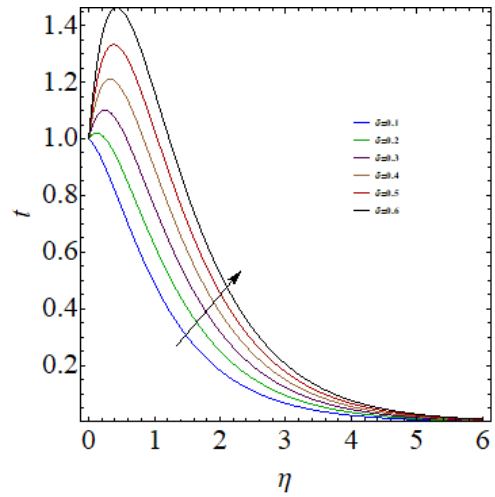

Figure 10. t via δ.

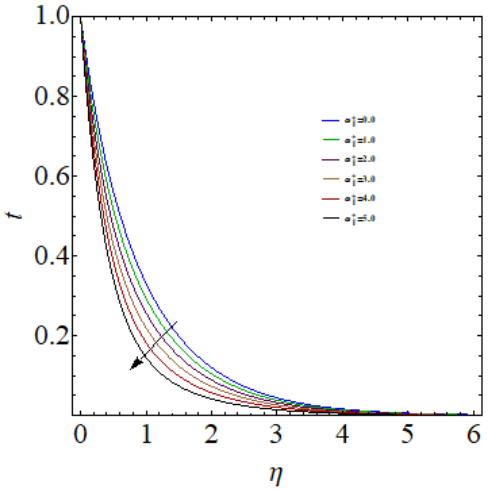

Figure 11. t via α_1^*.

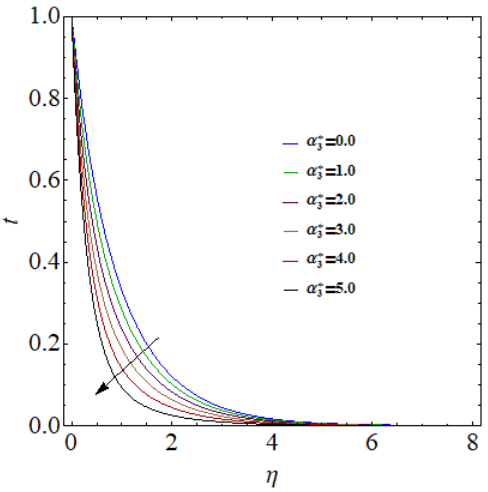

Figure 12. t via α_3^*.

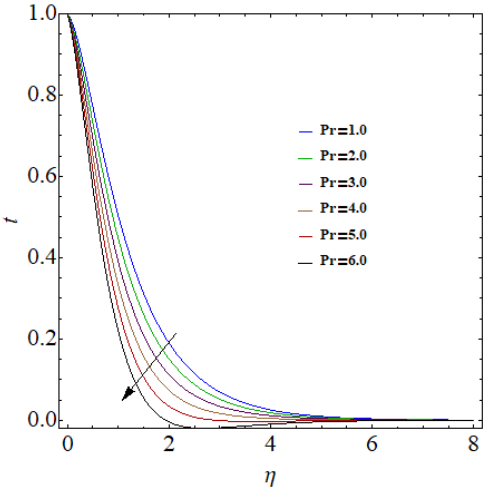

Figure 13. t via Pr.

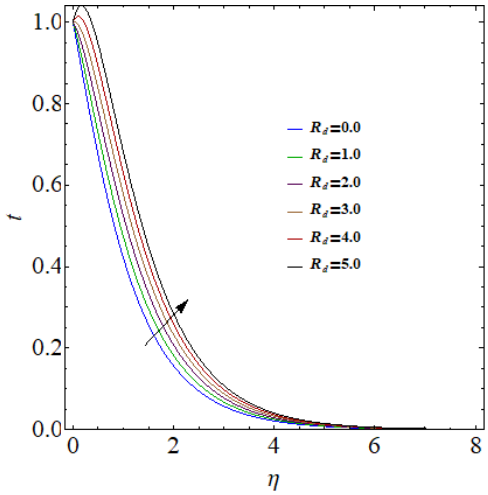

Figure 14. t via R_d.

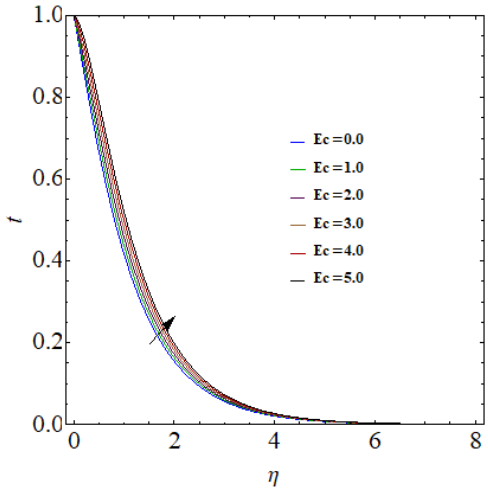

Figure 15. t via Ec.

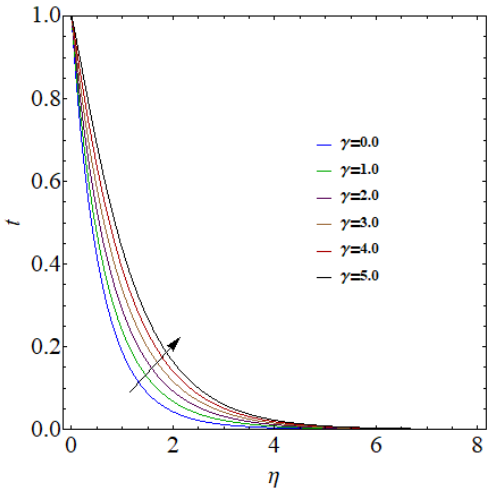

Figure 16. t via γ.

6.3 Nano-particles concentration:

Figure 18 reveals that the concentration $J(\eta)$ decreases with an increase in the Brownian motion parameter N_B. Physically, a higher N_B intensifies molecular collisions within the fluid, leading to heat generation that, in turn, reduces concentration. The influence of the thermophoresis parameter $N_T = 0.1, 0.2, 0.3, 0.4, 0.5, 0.6$ on $J(\eta)$ is examined in Figure 19, showing a notable increase in concentration

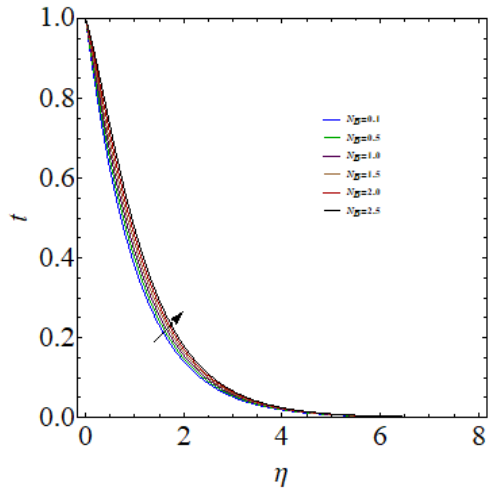

Figure 17. t via N_B.

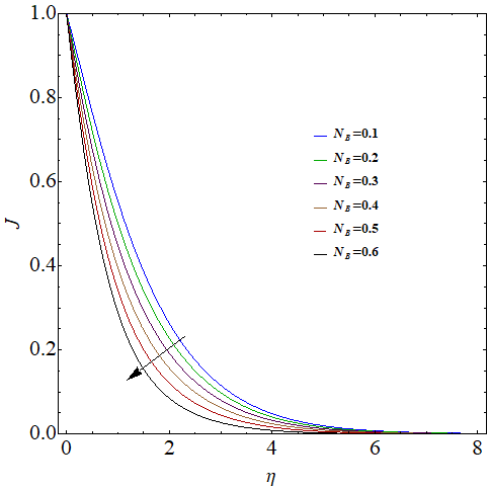

Figure 18. J via N_B.

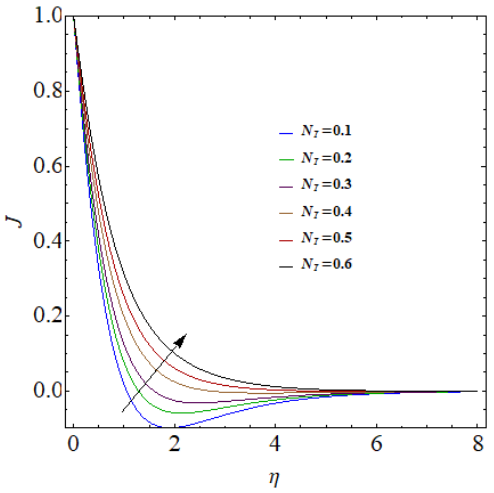

Figure 19. J via N_T.

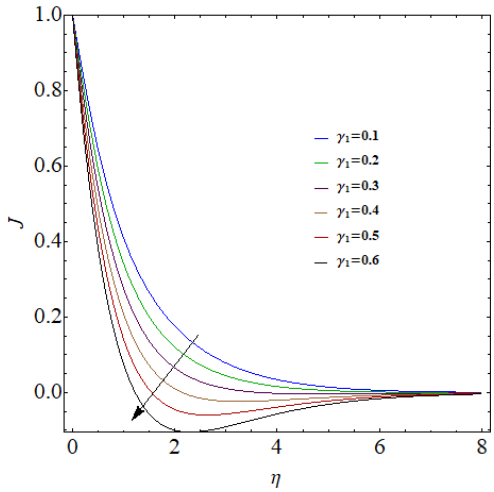

Figure 20. J via γ_1.

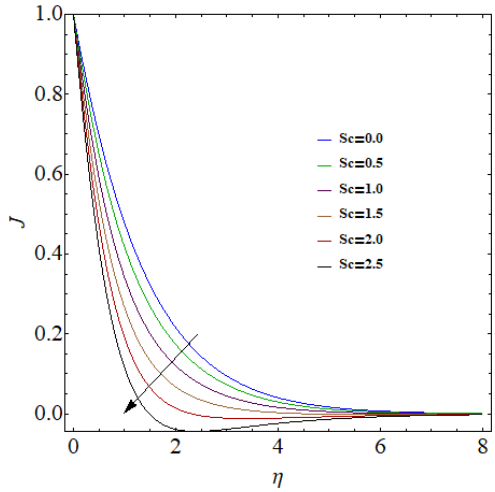

Figure 21. J via Sc.

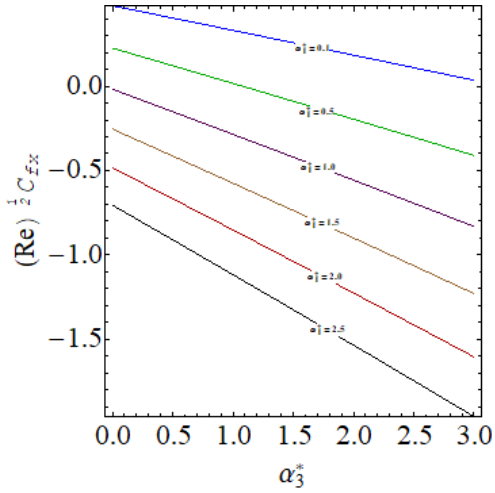

Figure 22. C_f via α_1^* and α_3^*.

as N_T rises. Figure 20 illustrates the effect of the mass relaxation parameter γ_1, where higher values of γ_1 reduce mass transfer from the fluid to the surface, resulting in a decline in $J(\eta)$. Figure 21 indicates that the concentration profile also decreases with increasing Schmidt number Sc, due to reduced mass diffusivity. Figure 22 shows the downward trend in wall shear stress with respect to the material parameters α_1^* and α_3^*; this occurs as their increase leads to greater resistance at the wall, lowering shear

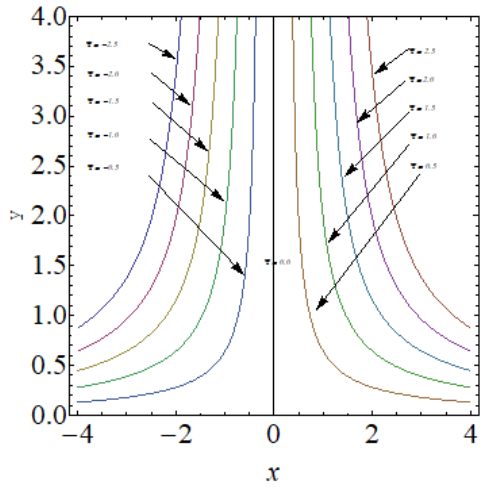

Figure 23. Streamlines for the flow.

stress. Figure 23 presents the streamline structure of the current flow field, providing insight into the flow behavior. Lastly, Table 1 lists the average squared residual errors corresponding to the optimal convergence control factor $\varepsilon^J_{k*} = 2$. The results confirm that residual errors decrease as the order of approximation increases, validating the convergence of the proposed solution.

7 Concluding remarks

In this study, a comprehensive numerical investigation has been carried out to explore the behavior of nonlinear third-grade nanofluids under generalized heat and mass flux conditions in a mixed convective flow regime. The results highlight the significant influence of fluid nonlinearity, nanoparticle concentration, and relaxation parameters on the thermal and concentration boundary layers.

The following are the main results:

1. M, α_1^*, α_2^* and α_3^* are the higher estimations of the fluid velocity while reduces via Da^{-1}.
2. For higher radiation and thermal relaxation parameters fluid temperature enhances.
3. Higher α_1^* and α_3^* lead to a rise in temperature.
4. Through (γ_1) and (Sc) concentration reduces.
5. Drag force is reducing for larger estimation of α_1^* and α_3^*.

Data Availability Statement

Data will be made available on request.

Funding

This work was supported by Jiangsu Excellent Postdoctoral Program under Grant 2023ZB890.

Conflicts of Interest

The author declares no conflicts of interest.

Ethical Approval and Consent to Participate

Not applicable.

References

[1] Fosdick, R. L., & Rajagopal, K. R. (1980). Thermodynamics and stability of fluids of third grade. *Proceedings of the Royal Society of London. A. Mathematical and Physical Sciences, 369*(1738), 351-377. [Crossref]

[2] Adesanya, S. O., & Makinde, O. D. (2015). Thermodynamic analysis for a third grade fluid through a vertical channel with internal heat generation. *Journal of Hydrodynamics, 27*(2), 264-272. [Crossref]

[3] Ellahi, R., & Riaz, A. (2010). Analytical solutions for MHD flow in a third-grade fluid with variable viscosity. *Mathematical and Computer Modelling, 52*(9-10), 1783-1793. [Crossref]

[4] Hayat, T., Nazar, H., Imtiaz, M., Alsaedi, A., & Ayub, M. (2017). Axisymmetric squeezing flow of third grade fluid in presence of convective conditions. *Chinese Journal of Physics, 55*(3), 738-754. [Crossref]

[5] Sajid, M., Mughees, M., Ali, N., & Shahzad, H. (2019). A theoretical analysis of blade coating for third-grade fluid. *Journal of Plastic Film & Sheeting, 35*(3), 218-238. [Crossref]

[6] Hayat, T., Naz, R., Asghar, S., & Mesloub, S. (2012). Soret–Dufour effects on three-dimensional flow of third grade fluid. *Nuclear engineering and design, 243*, 1-14. [Crossref]

[7] Choi, S. U., & Eastman, J. A. (1995). *Enhancing thermal conductivity of fluids with nanoparticles* (No. ANL/MSD/CP-84938; CONF-951135-29). Argonne National Lab.(ANL), Argonne, IL (United States).

[8] Buongiorno, J. (2006). Convective transport in nanofluids. [Crossref]

[9] Hayat, T., Shah, F., Khan, M. I., Khan, M. I., & Alsaedi, A. (2018). Entropy analysis for comparative study of effective Prandtl number and without effective Prandtl number via γAl2O3-H2O and γAl2O3-C2H6O2 nanoparticles. *Journal of Molecular Liquids, 266*, 814-823. [Crossref]

[10] Ahmad, S., Khan, M. I., Hayat, T., Khan, M. I., & Alsaedi, A. (2018). Entropy generation optimization and unsteady squeezing flow of viscous fluid with five

different shapes of nanoparticles. *Colloids and Surfaces A: Physicochemical and Engineering Aspects, 554*, 197-210. [Crossref]

[11] Fourier, J. B. J. (1888). *Théorie analytique de la chaleur*. Gauthier-Villars et fils.

[12] Cattaneo, C. (1948). Sulla conduzione del calore. *Atti Sem. Mat. Fis. Univ. Modena, 3*, 83-101.

[13] Christov, C. I. (2009). On frame indifferent formulation of the Maxwell–Cattaneo model of finite-speed heat conduction. *Mechanics research communications, 36*(4), 481-486. [Crossref]

[14] Ciarletta, M., & Straughan, B. (2010). Uniqueness and structural stability for the Cattaneo–Christov equations. *Mechanics Research Communications, 37*(5), 445-447. [Crossref]

[15] Haddad, S. A. M. (2014). Thermal instability in Brinkman porous media with Cattaneo–Christov heat flux. *International journal of heat and mass transfer, 68*, 659-668. [Crossref]

[16] Yusuf, A., Bhatti, M. M., & Khalique, C. M. (2025). Computational study of the thermophysical properties of graphene oxide/vacuum residue nanofluids for enhanced oil recovery. *Journal of Thermal Analysis and Calorimetry, 150*(1), 771-783. [Crossref]

[17] Shah, F., Fall, I., & Zhang, D. (2025). Breakage and coalescence mechanisms in multiphase flow comprehensive PBM-CFD review with turbulence modelling insights for gas-liquid system. *International Communications in Heat and Mass Transfer, 165*, 109093. [Crossref]

[18] Shah, F., Zhang, D., & Geng, L. (2025). A computational review of various inter-facial forces in fully developed multiphase fluid under different flow patterns in vertical column. *Propulsion and Power Research*. [Crossref]

[19] Ahmad, A., Asghar, S., & Afzal, S. (2016). Flow of nanofluid past a Riga plate. *Journal of Magnetism and Magnetic materials, 402*, 44-48. [Crossref]

[20] Liao, S. (2012). *Homotopy analysis method in nonlinear differential equations* (Vol. 153). Beijing: Higher education press. [Crossref]

[21] Sheikholeslami, M., Hatami, M., & Ganji, D. D. (2013). Analytical investigation of MHD nanofluid flow in a semi-porous channel. *Powder Technology, 246*, 327-336. [Crossref]

[22] Zheng, L., Wang, L., & Zhang, X. (2011). Analytic solutions of unsteady boundary flow and heat transfer on a permeable stretching sheet with non-uniform heat source/sink. *Communications in Nonlinear Science and Numerical Simulation, 16*(2), 731-740. [Crossref]

[23] Hayat, T., Shah, F., Hussain, Z., & Alsaedi, A. (2018). Outcomes of double stratification in Darcy–Forchheimer MHD flow of viscoelastic nanofluid. *Journal of the Brazilian Society of Mechanical Sciences and Engineering, 40*(3), 145. [Crossref]

Faisal Shah is currently a Post Doc Fellow in National Research Center of Pumps, Jiangsu University China. He received his Ph.D. degree from Quaid-i-Azam University in 2021. His research interests include Applied mathematics, Fluid dynamic, multiphase flow and the optimization of fluid machinery. He is published 46 research articles in various international journals. (Email: sfaisal@math.qau.edu.pk)